Computer-Optimization of Vascular Trees

Wolfgang Schreiner and Peter Franz Buxbaum

Abstract—**Arterial branchings closely fullfil several "bifurcation rules" which are deemed to optimize blood flow. The question is whether these local criteria in conjunction with a general optimization principle can explain the overall structure of an arterial tree. We present a model of an arterial vascular tree which is grown on the computer by successively adding terminal vessel segments. Each new terminal segment is connected to the optimum site within the preexisting tree, and the new bifurcation is optimized geometrically. After each step of adding and optimizing, the whole tree is rescaled to meet invariant boundary conditions of pressure and flow at each terminal site. Thus, local geometric optimization is used to induce simultaneously an optimized global structure. The comparison between the model and real coronary arterial trees shows good agreement regarding structural appearance, morphometric parameters, and pressure profiles.**

I. Introduction

ARTERIES serve the purpose of conveying blood to the tissue and thus provide a key precondition for metabolism ("perfusion task"). The complex structure of arterial trees raises the question why vessels run and bifurcate the way they do, and if there are any underlying optimization principles which might induce, or even necessitate the structures actually found.

Stereometric measurements on corrosion casts of human coronary arterial trees [1] have revealed that arterial bifurcations indeed obey certain "bifurcation rules" in the sense that ratios of vessel radii, branching angles, and the splitting of blood flow closely follow mathematical relations among each other [2], [3]. These relations are also physiologically reasonable. For example, segment radii may shrink at bifurcations so as to enable uniform shear stress between blood and vessel walls [4] or else to facilitate pulse wave propagation [5]. Clearly, such findings have to be incorporated in a model.

In addition, several theoretical criterions ("target functions") related to functional optimality of arterial trees have been proposed [6] and even weighted combinations were considered [7]. Since none of these targets can be strictly proved to be "the most adequate," we select a most simple candidate: the blood volume inside the vessel tree should be as small as is consistent with the perfusion task to be fulfilled. This choice of target function is

1. Physiologically reasonable [6], since blood is a substance expensive for the organism to maintain.
2. It is suitable to demonstrate the feasibility of our simulation method. And last not least
3. For an *isolated* bifurcation it has already been shown that its geometric location can be optimized according to minimum volume as a target function T, provided that the geometric locations, pressures and flows are given for the inlet of the parent (feeding) segment and for both outlets of the daughter (draining) segments [6]. In other words: searching for minimum volumes makes the minimization routine converge nicely.

However, despite the finding that reasonable "bifurcation rules" are locally fulfilled in real arterial trees and that isolated model bifurcations can be optimized, it remained an open question whether the line of argument could be inverted: Is the *overall* structure of an arterial tree the necessary consequence of an optimization principle and how can it be derived or constructed?

In the current study we present a computational method which optimizes single bifurcations geometrically and simultaneously induces an optimal connective (topological) structure in a growing vessel tree. Both geometric and topological optimization are governed by minimizing the same target function, namely the total blood volume inside the vessel tree [6]. Throughout the growing of the model tree, boundary conditions of pressure and flow are imposed so as to represent physiologic conditions. Accordingly, the model tree offers optimized functionality not only in its fully developed form but also at each intermediate state of development. This suggests analogy to the development of living systems.

II. Model Objectives, Specification, and Requirements

A. Nomenclature of Binary Tree Model

Large arteries and major side branches can be labelled in terms of topographic anatomy (e.g., main left, left anterior descending coronary artery [8], etc.). However, the number of vessels increases drastically as one proceeds towards smaller diameters. Then topographical labelling has to be replaced by a statistical description such as the "segmental analysis" performed by ZAMIR and CHEE [1] on corrosion casts of human coronary arteries. The nomenclature used in that experimental work is expanded to the present needs such that compatibility is retained and results may be compared.

The arterial tree is decomposed into "segments," i.e., intervals of vessels between two consecutive bifurcations [1]. Each segment is assigned four integer numbers: 1) its own unique segment index i, 2) a backward pointer B_i holding the index of its parent (feeding) segment, and 3) the pointers D_i^l and D_i^r to

Manuscript received September 5, 1991; revised March 24, 1992. The work was supported by the Ludwig Boltzmann Institut für Herzchirurgische Forschung.

The authors are with the 2nd Department of Surgery, Working Group for Biomedical Computersimulation University of Vienna, A-1090 Wien, Austria.

IEEE Log Number 9205274.

left and right daughter, respectively. This whole set of numbers (redundantly) describes the connective-relations (topology) of the tree, see Fig. 1. Of note the root (main feeding artery) has no parent segment ($B_{i\text{root}}$ = "NIHIL"). In the model, each segment i is represented by a straight cylindrical tube of radius $r(i)$ and length $l(i)$, see Fig. 1, perfused according to Poiseuille's law [9]. In particular, we additionally define $r_{\text{root}} = r(i\text{root})$. If a segment bifurcates, bifurcation ratios ("left bifurcation ratio," "right b.r.")

$$\beta^l(i) = r(D_i^l)/r(i)$$
$$\beta^r(i) = r(D_i^r)/r(i) \tag{1}$$

are defined to characterize daughter radii in relation to the radius of the parent segment, $r(i)$. Bifurcations may be highly asymmetric (when a large vessel gives off a small branch) or perfectly symmetric ($\beta^l(i) = \beta^r(i)$). Note however, $\beta^{\cdot} < 1$ for arterial bifurcations. Repeated branchings and concomitant reductions in radii constitute a dichotomous (binary) tree of vessel segments, which in real arterial systems comprises arteries (radius > 1 mm), small arteries (1–0.1 mm) and arterioles (0.1–0.02 mm). At the arteriolar level, however, the topology of real arterial systems switches from a dichotomous tree to arcade networks [10], [11], featuring crosslinks between vessels, unifications and glomerulies, characteristic also for the capillary bed. The prearteriolar level hence marks an ultimate and conceptual cutpoint at which the binary tree model has to be truncated in the form of "terminal segments," which are not parent to another bifurcation (pointers $D_i^l = D_i^r$ = "NIHIL," $\beta^l(i) = \beta^r(i)$ = "Undefined" if i is a terminal segment). Instead, all N_{term} terminal segments are assumed to perfuse equal areas of tissue, which are considered as "microcirculatory black-boxes" rather than being modeled in detail (hatched areas in Fig. 1).

The location (including orientation and length) of each segment is defined by the cartesian coordinates $(x(i), y(i))$ of its downstream (i.e., distal) end, together with the corresponding values of its parent, B_i. An exception is the root's inlet.

Trifurcations, sometimes seen in real arterial trees, are not considered in the model. However, a segment between successive bifurcations *may be very short*, which de facto resembles a trifurcation.

2. Perfusion Task and Constraints

The confined portion of tissue to be perfused (e.g., the anterior wall of the left ventricle of the heart) is modeled as a two-dimensional circular area ("perfusion-area" A_{perf}, radius r_{perf}). The main feeding artery, represented by the root segment of the model tree, is perfused at a pressure p_{perf} and carries the flow Q_{perf} as it enters the perfusion-area (Fig. 1). Total perfusion flow should finally be distributed evenly over the perfusion-area A_{perf}.

To these ends we consider A_{perf} being divided into N_{term} "subareas" of equal size, each of them corresponding to a microcirculatory black-box, and reformulate the key task of the model as follows: how shall a tree be designed in order to supply all microcirculatory black-boxes with equal flows

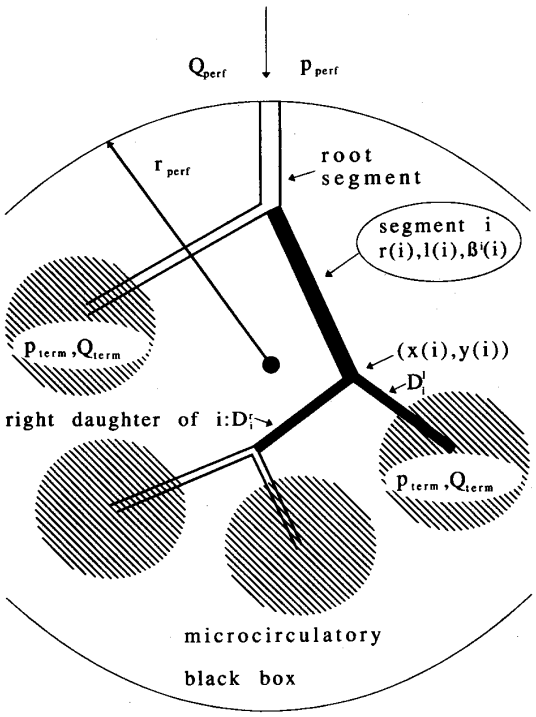

Fig. 1. Nomenclature for the binary tree model. Blood flow Q_{perf} enters root segment at pressure p_{perf}. Microcirculatory blackboxes (hatched circles), distributed over the perfusion area (radius r_{perf}) receive equal flows (Q_{term}) at equal pressures, p_{term}. Segment i with left and right daughter segments (pointers: D_i^l, D_i^r), shown in solid fill. Left daughter is terminal, supplying a blackbox, the right daughter branches into a subtree. (x_i, y_i) are coordinates of downstream end of segment. Schematic, nonquantitative display.

(Q_{term}) at equal pressure (p_{term}) and at the same time minimize a target function such as, e.g., the total blood volume inside the tree [6]? In order to guarantee realistic bifurcation conditions, we additionally have to impose a "bifurcation rule" of the form

$$r^{\gamma}(i) = (r(D_i^l))^{\gamma} + (r(D_i^r))^{\gamma}. \tag{2}$$

Although this form of law is unquestioned, several values for the parameter γ ("bifurcation exponent") have been reported. Direct measurements at bifurcations [12] suggested $\gamma = 3.00$, corresponding to a necessary (but not sufficient) condition for equal shear stress between blood and the vessel walls in the feeding and draining branches [4]. Conversely, $\gamma = 2.55$ was obtained indirectly by counting the number of distal branches, and guarantees a minimum reflection of pulse waves [5]. Regardless of the particular value of γ, provided it is constant throughout the tree, (2) makes the bifurcation ratio (1) a redundant quantity.

C. Desired Features and Final Aim

While fulfilling the above mentioned conditions, the model should yield both i) the connective relations (topology, branch-

ing pattern) and ii) quantitative geometric results (coordinates and radii) for all segments of the tree. This implies several features of the model:

1. The overall resistance of the resulting model tree will produce the required pressure drop $p_{\text{perf}} - p_{\text{term}}$ at the prespecified perfusion flow, Q_{perf}.
2. The pressure drop along the path from the root to any of the microcirculatory black-boxes is the same for all terminal segments.
3. The flow Q_i through a segment is proportional to the number of distal microcirculatory black-boxes, NDIST_i: $Q_i = \text{NDIST}_i \cdot Q_{\text{term}}$. For a terminal segment, $\text{NDIST}_i = 1$ by definition.
4. Due to the binary mode of branching, a tree with N_{term} terminal segments has $N_{\text{tot}} = 2 \cdot N_{\text{term}} - 1$ segments in total, regardless of its particular structure.

III. Generating the Optimized Model Tree

Modeling all vessel segments of the left coronary circulation down to the prearteriolar level would by far exceed the computational resources presently at hand. Hence, we have to preset a manageable number of terminal segments and thus truncate the model well before its conceptual cutpoint, where structure switches from binary to arcade networks. Parts of a real tree, which are still dichotomously branching, will then be lumped into the microcirculatory black-boxes.

A crude but simple approach of generating an optimized tree could then proceed as follows: the distal ends of all terminal segments are distributed evenly over the perfusion area. Then all possible trees (i.e., connective structures), one after the other, could be constructed and geometrically optimized to minimum blood volume for each given structure. Finally, one would adopt that structure which had been optimized to the smallest blood volume. Despite being feasible, as will be shown later, this approach is computationally exceedingly expensive. A few hundred terminal segments would be the utmost complexity manageable.

Instead we generate and simultaneously optimize the model tree in a *stepwise* fashion, which imitates the growth of a real arterial tree and is also fast enough to cope with several thousand segments.

A. Planting the Root

Initially, the perfusion-area is scaled down to a small supporting circle (radius r_{supp}), whose area equals that of one "microcirculatory black-box" ($\pi \cdot r_{\text{supp}}^2 = A_{\text{perf}}/N_{\text{term}}$). The root segment is then generated with its proximal end at the circle border and the distal end selected randomly within the supporting circle. According to the resulting segment length, the radius (r_{root}) is chosen such that the resistance (according to Poiseuille's law) yields the flow Q_{term}, appropriate for one microcirculatory black-box. The result is a degenerate tree, comprising only one segment (which is the root and at the same time terminal). Yet the tree is "scaled" (has a total resistance and flow consumption adequate for the number of terminal segments to be supplied, $k_{\text{term}} = k_{\text{tot}} = 1$).

Without loss of generality we may now assume that a tree of k_{term} terminal segments has already been generated. Then the next terminal segment is added in several steps, as follows.

B. Inflating the Real World Parameters (Supporting Circle)

The perfusion area (radius r_{supp}) is increased to $(k_{\text{tot}}+1) \cdot A_{\text{perf}}/N_{\text{tot}}$, so as to accommodate the area of one additional black-box. The coordinates of all segments are stretched correspondingly. The resulting increase in segment lengths is compensated by increasing all radii in order to rescale the whole tree to correct total resistance. Of note the computer program works in reduced units, and model parameters are converted to real world values via r_{supp} as scaling factor.

C. Adding a Terminal Segment

The coordinates for the distal end of a new terminal segment are selected by generating pseudorandom numbers, uniformly distributed in x and y direction inside the supporting circle. For a prospective location (x, y), the distance to each of the preexisting segments is calculated as follows: Let $(x(j), y(j))$ denote the distal and $(x(B_j), y(B_j))$ the proximal end of an existing segment, j. We first formulate a criterion to decide if (x, y) lies "somewhere along segment j" or rather close to one of its endpoints:

$$d_{\text{proj}}(x,y,j) = \begin{pmatrix} x(B_j) - x(j) \\ y(B_j) - y(j) \end{pmatrix} \cdot \begin{pmatrix} x - x(j) \\ y - y(j) \end{pmatrix} \cdot l(j)^{-2} \quad (3)$$

where "·" between vectors denotes the scalar product. If $0 \le d_{\text{proj}} \le 1$, the projection lies within segment j. In this case the orthogonal distance is considered crucial and calculated as

$$d_{\text{crit}} = d_{\text{ortho}}(x,y,j) = \left| \begin{pmatrix} -y(B_j) + y(j) \\ x(B_j) - x(j) \end{pmatrix} \cdot \begin{pmatrix} x - x(j) \\ y - y(j) \end{pmatrix} \right| \cdot l(j)^{-1}. \quad (4)$$

For other values of d_{proj}, the orthogonal distance is certainly uncritical, however, the distance between (x, y) and one of the endpoints of segment j may still be critical and is obtained as

$$\begin{aligned} d_{\text{crit}} &= d_{\text{end}}(x,y,j) \\ &= \text{Min}\{((x - x(j))^2 + (y - y(j))^2)^{1/2}, \\ &\quad ((x - x(B_j))^2 + (y - y(B_j))^2)^{1/2}\}. \end{aligned} \quad (5)$$

If d_{crit} thus obtained exceeds a threshold distance, d_{thresh}, (x, y) is accepted to become the location of the distal end of the next terminal segment to be added, otherwise tossing for new coordinates is repeated N_{toss} times. Should it still fail, d_{thresh} is multiplied by 0.9 and the process repeated until an acceptable (x, y) is obtained. Prior to each lap of adding a new terminal segment, the threshold is reinitialized with

$$d_{\text{thresh}} = (\pi \cdot r_{\text{supp}}^2 / k_{\text{term}})^{1/2}. \quad (6)$$

This adaptive process of tossing for terminal locations favors regions with low density of existing segments and thus leads to an even distribution of microcirculatory black-boxes over the

perfusion area. Similar to the growth of real vascular trees, the formation of new vessels is demand-induced within the model.

Next, a key question arises: to which of the preexisting segments shall the new one be connected? The answer determines the topology of the tree. For reasons of clarity, we relegate this "connection search" to a later section and first treat the problem of *how* to connect a terminal segment to an arbitrary preexisting segment, labeled i_{conn}.

The segment i_{conn} is detached from its parent, i_{old}, and (arbitrarily) shortened to half its length, the distal end being unaffected, see its "empty filled" portion in Fig. 2. A new (bifurcating) segment, i_{bif}, is inserted (shown in solid fill), having i_{old} as parent and i_{conn} and i_{new} as daughter segments. Next, the flow splitting at bifurcation i_{bif} has to be adjusted so as to yield Q_{term} toward the new terminal segment i_{new}, and the flow $\text{NDIST}_{i_{\text{conn}}} \cdot Q_{\text{term}}$ into the subtree distal to i_{conn}. First, we note that the total resistance of this subtree is proportional to the fourth inverse power of the inlet radius ($[r(i_{\text{conn}})]^{-4}$), provided that all segment lengths and bifurcation ratios within the subtree remain unchanged. The same is true for the new terminal segment i_{new}, which can be considered as a degenerate subtree. Consequently, the *relative resistances and thus flow splitting* can be completely controlled and adjusted as required via the ratio $r(i_{\text{conn}})/r(i_{\text{new}})$. Using the bifurcation rule (2), $r(i_{\text{bif}})$ and the bifurcation ratio $\beta^l(i_{\text{bif}})$ are obtained. As a result, flows split correctly within the subtree distal to i_{bif}, and the subtree's resistance is again proportional to the fourth inverse power of its inlet radius, $(r(i_{\text{bif}})^{-4})$. This procedure is labelled "balancing of the bifurcation ratio." However, since an additional terminal segment is now to be supplied via the left daughter of i_{old} (see Fig. 2), the bifurcation ratio $\beta^l(i_{\text{old}})$ must be rebalanced. The same is true for all bifurcations proximal to i_{bif}, since one of their daughters has to accommodate the additional flow through the new terminal segment. This recursive procedure, starting at i_{bif}, is called "balancing bifurcation ratios up to the root." Finally, r_{root} is rescaled to make the whole tree yield a total flow of $(k_{\text{term}}+1)\cdot Q_{\text{term}}$. This we label "scaling" of the tree. Of note in the computer program, only bifurcation ratios rather than absolute values of radii are considered. An exception is r_{root}, which in fact scales all radii via bifurcation ratios and (2).

D. Geometric Optimization

After connecting a new terminal segment, the target function T for optimization, e.g., the volume of the whole tree, is evaluated. Of note T depends on the location $(x(i_{\text{bif}}), y(i_{\text{bif}}))$ of the new bifurcation, chosen rather arbitrarily at half way within the former segment i_{conn} (see Fig. 2). Small incremental changes of $x(i_{\text{bif}})$ and $y(i_{\text{bif}})$, each followed by "rebalancing up to the root" and "scaling," are used to estimate the gradient $\vec{\nabla}T = (\partial/\partial x(i_{\text{bif}}), \partial/\partial y(i_{\text{bif}}))T$ of the target function. The bifurcation is then repeatedly moved [13] along descending gradient, ending up with a geometric optimization of the new bifurcation (cf. Fig. 2). The final value of the target function, $T(i_{\text{new}}, i_{\text{conn}})$, represents the best result attainable when choosing the segment i_{conn} as the connection site for the new terminal segment, i_{new}.

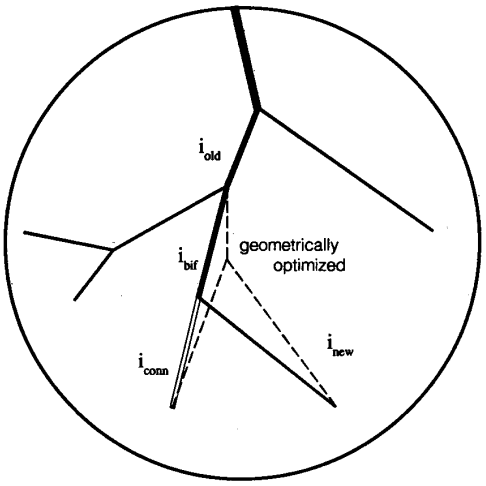

Fig. 2. Adding a Terminal Segment. A preexisting tree of k_{term} segments is assumed to be balanced and scaled. Segment i_{conn} is the selected site for connection of the new terminal segment, i_{new}. i_{conn} is shortened (empty section) and the new bifurcation, i_{bif}, is inserted (solid fill) and its coordinates are geometrically optimized (dashed).

E. Removing a Bifurcation

The new bifurcating segment, inserted to supply a new terminal branch, can also be removed again: The segment i_{conn} is stretched backwards to its original length, the proximal end being reattached to i_{old}. The segments i_{bif} and i_{new} are discarded, all bifurcation ratios from i_{old} up to the root are rebalanced and the tree is scaled, thus restoring exactly the situation before adding.

F. Connection Search

With tools available for creating, optimizing, and removing the connection of a new terminal segment, we now return to the question, which of the preexisting k_{tot} segments should be selected for the connection (i.e., play the role of i_{conn}). The answer is now quite simple.

The new terminal segment is connected to each of the preexisting segments, one after the other. Each time the generated bifurcation is geometrically optimized, the corresponding values of the target function and bifurcation coordinates are stored, and the bifurcation is removed again. A connection is further ignored, if the new terminal segment intersects with any other segment of the tree, except for i_{bif} and i_{conn}. That segment found to yield the lowest minimum for the target function, is finally adopted (with its coordinates optimized) to provide the actual and lasting connection. This step, while being governed by the target function, induces the connective relationships (topology) within the tree and closes the process of "growing the tree" by one additional terminal segment.

Again we recall that local geometric optimization of tentative connections is a basis to precede the global search for optimized connective structure. In the model, topology is "grown in an optimized way" as terminal segments are successively added until the tree is finished.

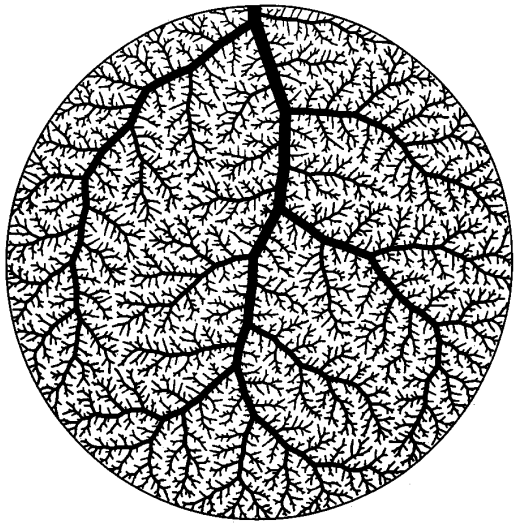

Fig. 3. Tree with 4000 terminal segments. Full optimization for minimum volume. Computing time around two days on an IBM 3090 mainframe.

IV. Results

A. Highly Detailed Model of a Coronary Artery Tree

The above simulation method has been presented in general terms, since there are only four main determinants deciding upon the structure obtained:

1. The total number of terminal segments, N_{term}, determines the grade of detail (finess) represented in the model and is primarily a question of computer resources available. We choose $N_{\text{term}} = 4000$, which takes about two days of execution time on an IBM 3090 mainframe with a vector facility.
2. The "bifurcation exponent" γ, governing the shrinkeage of radii across bifurcations.
3. The target function, T, to be optimized.
4. The sequence of pseudorandom numbers used for tossing (NAG Library ®, Numerical Algorithms Group Ltd), and the algorithm applied for selecting those positions acceptable as locations of terminal segments (see section "Adding a Terminal Segment").

The particular values chosen for further parameters such as pressures, flows, size of tissue and the viscosity of blood *merely* scale *the radii of all* segments but do not affect the tree's structure (except for some very tiny side-branches given off by major branches). Yet, when generating a highly detailed tree in order to demonstrate the feasibility of the simulation concept, we prefer selecting "realistic" parameter values (see next section and Table I). Thus, the segment radii obtained are in proper (i.e., realistic) relation to the total size of the perfusion area (Fig. 3).

B. Inserting "Real World Parameters"

In order to simulate a particular vascular bed, parameters for pressures and flows need to correspond to the real situation, see Table I. We choose this to be a coronary arterial bed similar to that of the *left anterior descending (LAD) coronary artery in humans,* regarding flow, size, pressures and mass of tissue.

The perfusion area should mainly represent the anterior wall of the left ventricle, and r_{perf} is set at 5 cm (8). Total perfusion flow, Q_{perf}, is set at 500 mL/min, referring to a nonbeating heart in a vasodilated state as follows. The LAD coronary artery supplies approximately 100 g of myocardial tissue, each gramm requiring a flow of 1 mL/min [14] (normal, resting conditions). Vasodilation is assumed to increase this reference flow through the LAD bed (100 mL/min) to 300 mL/min [15]. Coronary flow additionally increases if the heart is arrested, since the flow-impeding effect that myocardial compression exerts on the microcirculation is absent. Experimental data [16] and mathematical models [17], [18]) indicate this increase to range between 40% and 70%. Thus one arrives at approximately five times the normal flow and we set $Q_{\text{perf}} = 500$ mL/min.

TABLE I
Predefined Model Parameters. The Vascular Bed of the Left Anterior Descending (LAD) Coronary Artery is Assumed to Perfuse 100 g Myocardial Tissue. Perfusion Flow Q_{perf} (1 mL/min/100 g Normal Conditions, Beating Heart) is Increased Five-fold to Represent Nonbeating Vasodilated Conditions. To Obtain Constant Diameter of the Root Segment, Terminal Pressure p_{term} Must Decrease with Increasing Number of Terminal Segments N_{term}.

Symbol	Meaning	SI-Units (conventional)	Source
N_{term}	number of terminal segments	250–4000	preset for each run
R_{perf}	radius of circular area representing tissue to be perfused (LAD region)	0.05 m (5 cm)	Ref. [8]
Q_{perf}	LAD flow in vasodilated non-beating heart	$8.33 \cdot 10^{-6}$ m^3/s (500 mL/min)	Ref. [8], [16] [15], [17], [18]
p_{perf}	perfusion pressure	$1.33 \cdot 10^4$ Pa (100 mmHg)	Ref. [8], [30]
p_{term}	pressure at distal ends of terminal segments:		Ref.[30]
	for $N_{\text{term}} = 250$:	$8.38 \cdot 10^3$ Pa (63 mmHg)	
	= 4000:	$7.98 \cdot 10^3$ Pa (60 mmHg)	
η	viscosity of blood (assumed as constant)	$3.6 \cdot 10^{-3}$ Pa · s (3.6 cP)	Ref. [38]
γ	bifurcation exponent [defined in (2)]	2.10–3.00	Ref. [5], [12]

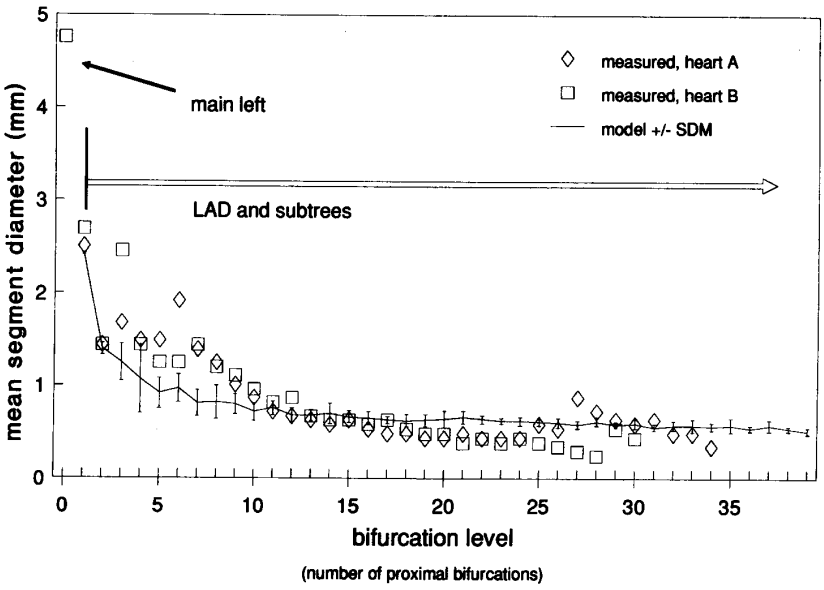

Fig. 4. Morphometric comparison between model and the left coronary artery trees of two humans. Vertical axis: averaged segment diameter. Horizontal axis: bifurcation level (= number of proximal bifurcations). Measurements from corrosion casts (1) of the left coronary circulation of two human hearts (symbols ◇ and □). Model simulations with 250 terminal branches (499 in total) refer to the LAD (or LCX) bed only and hence start at level 1 (polygon curve). Vertical bars represent standard deviations of means obtained from 10 model replicates with identical parameters (Table I), using different pseudo-random numbers, however. Computation time about 15 min per run.

For the perfusion pressure at the entrance of the root segment a representative value for mean arterial pressure is chosen ($p_{\mathrm{perf}} = 100$ mmHg).

An issue deserving more detailed coverage is the setting of p_{term}, being the (unique) pressure at the distal ends of all terminal segments. Clearly, as one proceeds through an arterial tree downstream into smaller branches, pressure declines. Consequently, if a model tree features more terminal segments, these will be generally smaller and hence p_{term} should be lower. In order to evaluate the proper dependence of p_{term} on N_{term}, simulations were performed for increasing values of N_{term}, using the same (tentative) value of p_{term}, say 60 mmHg. As expected, the root's radius (r_{root}) was seen to increase slightly, so as to maintain a constant perfusion flow (Q_{perf}) through an increasingly complex tree. On the other hand, each model of a given arterial bed should yield the same r_{root}, regardless of its particular complexity. This can be achieved by adjusting p_{term} so as to "rescale" trees with different N_{term} to have equal r_{root}. The dependence thus found was rather small over a wide range of N_{term}: if $p_{\mathrm{term}} = 60$ mmHg is used for $N_{\mathrm{term}} = 4000$, then 63 mmHg applies to $N_{\mathrm{term}} = 250$, see Table I.

C. Morphometric Comparison With Real Coronary Arterial Trees

Zamir and Chee [1] used corrosion casts to perform a morphometric analysis of the coronary arterial trees in two human hearts. They classified each vessel segment according to the number of proximal bifurcations ("bifurcation-level"), measured the diameter, and displayed average diameters versus bifurcation-level (◇, □, Fig. 4). For comparison, an optimized model tree was generated and then analyzed along the same lines (Fig. 4). In order to reduce systematic differences between the three-dimensional geometry of the heart and the two-dimensional model, the simulation was restricted to the tree of the left anterior descending (LAD) coronary artery, rather than covering the left ventricle as a whole. Note that the LAD orifice has level 1 in a tree starting with the main left coronary artery (level 0), see Fig. 4.

The stability of results was assessed via ten replicates of the model tree, each using a different sequence of pseudorandom numbers for casting the distal ends of its terminal segments. For each replicate diameters were averaged within each level. The standard deviations of these mean diameters are shown as vertical bars in Fig. 4, the averages over replicates are joined by the polygon line.

Close agreement with measurements is found for the models' root diameters (level 1), for level 2 and for levels higher than 10. Discrepancies between levels 3 and 10 may either indicate that our optimization concept is inappropriate for branchings close to the root of a tree. Or else small sidebranches, supplying tissue adjacent to the root, were considered in the model while being lost from the corrosion casts, e.g., due to their mechanical fragility. Note however, that the diameters of a small sidebranch and the main vessel's continuation are averaged within the same level, yielding a mean value significantly below the main vessel's diameter.

D. Comparing the Pressure Profile With Experimental Measurements

Microvascular pressures within the coronary circulation have been measured in cats [19], [20], rabbits [21], and rats

[22]. For a reasonable comparison between the model and experimental measurements, e.g., the most comprehensive and recent data reported by Chilian [19], it is necessary to i) express all pressures as percent of aortic pressure [23] and ii) scale the model to the dimensions, flow, and mass of a cat's LAD perfusion area.

The radius of the perfusion area, $r_{\text{perf}} = 1.25$ cm, is set to half the enddiastolic diameter of a cat's heart [24]. The mass of tissue is assumed to comprise one third of the total heart [25] (15 g/3 = 5 g), being perfused by a flow of 32 mL/min (measured: 6.42 mL/min/g under dipyridamole induced vasodilation, see [19]). Terminal pressure p_{term}, was set at 35 mmHg, representing the conditions in small arterioles [26]. Perfusion pressure is set at 100 mmHg, and hence absolute values for pressures within the model numerically equal percentages of perfusion pressure.

Note that such a rescaling does not change the structure of a model tree and also preserves relative segment lengths and radii. Rescaling the model tree displayed in Fig. 3 to the cat's conditions, yields a root segment's radius of 0.38 mm, slightly below the range for a cat's LAD diameter (0.8 to 1.2 mm).[1] Segments were classified according to radius [equidistant in log(radius)], and pressures at the distal ends of the segments within each class were averaged, see the dashed curves in Fig. 5. In contradiction to measured pressure profiles [19], too much resistance is seen to reside in the larger branches.

As a consequence of this finding, simulations were performed using values other than 3.00 for the parameter γ ("bifurcation exponent"), cf. (2). This *change of local bifurcation laws* proved to significantly change the pressure profile. For $\gamma = 2.10$ the profile is fairly flat across the larger branches, growing steeper towards smaller radii (dotted curve in Fig. 5). Finally, for $\gamma = 2.55$ the profile is in reasonable agreement with measured data and also exhibits a quasi linear shape (in logarithmic display), being characteristic for the vasodilated state [26]).

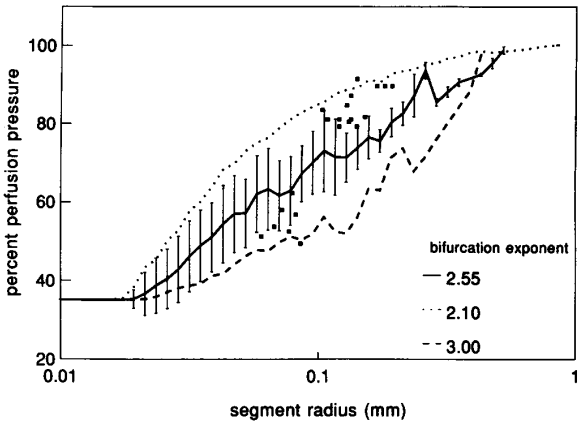

Fig. 5. Pressue profile and bifurcation laws. Pressures relative to aortic pressure (assumed 100 mmHg in the model). ■: Measurements in cat's left ventricle (19), vasodilation with dipyridamole, values relative to aortic pressure. For comparison, the model was run with 4000 terminal segments, scaled on a cat's LAD area. Changing the "bifurcation exponent" γ is seen to influence the profile: $\gamma = 2.55$ (solid curve with error bars denoting standard deviations of pressures), $\gamma = 2.10$ (dotted) and $\gamma = 3.00$ (dashed).

E. Residual Heterogeneity of Perfusion

Real coronary vascular beds exhibit a considerable variation in regional flows, both spatial and temporal. Perfusion heterogeneity is usually characterized by the coefficient of variation ($\text{CV}_{\text{flow}}(m)$ = standard deviation/mean) of flows into tissue samples of a given mass, m. These regional flows can be assessed via the deposition of labeled microspheres [27]. For example, Bassingthwaighte *et al.* [28] found the average $\text{CV}_{\text{flow}}(1\text{ g})$ to range between 0.15 (in baboons) and 0.21 (in sheep).

Seemingly opposed to this, *homogeneous* perfusion is aimed at within the model (by evenly distributing the distal ends of terminal segments). However, since homogeneous perfusion is an objective rather than a boundary condition, it is only approached but never fulfilled with a finite number of vessel segments. The "residual perfusion inhomogeneity" within the model can be evaluated either by a i) simulation of a microsphere deposition (so as to mimic the experimental procedure) or by ii) computing the variation in the density of terminal segments.

Microsphere deposition is simulated as follows. Given the microsphere radius, r_{ms}, the model tree is scanned for those locations where microspheres "get stuck." This is assumed to occur wherever a parent segment with radius $\geq r_{\text{ms}}$ gives off a daughter branch with radius $< r_{\text{ms}}$. If both daughters have radii $< r_{\text{ms}}$, two depositions are assumed. Counting the number of estimated deposition sites within a sampling area provides an estimate proportional to what is measured as regional flow into a sample of real tissue. The only drawback is that real microspheres usually are much smaller (around 16 μm) than any r_{ms} appropriate for the model, since r_{ms} must exceed the radii of all terminal segments (e.g., $r_{\text{ms}} \geq 200\,\mu$m for the tree in Fig. 3). As a consequence, as perfusion density is estimated on a more coarse-grained basis, inhomogeneity will be overestimated. In fact, we obtain $\text{CV}_{\text{flow}}(1\text{ g}) = 0.47$, which is at least twice as large as the experimental value. Please note that this estimate remains unchanged for increasing N_{term} (i.e., increasing model finess).

Alternatively, counting the number of terminal segments within areas corresponding to 1 g of tissue yields $\text{CV}_{\text{flow}}(1\text{ g}) = 0.16$, lying well within the range of experimental values [28]. However, this estimate has the disadvantage to depend on the finess (N_{term}) of the model. For example, in a model tree with $N_{\text{term}} = 1000$, $\text{CV}_{\text{flow}}(1\text{ g})$ increases to 0.3.

Using either calculation method, the estimate of CV depends on the mass of sample, m. log (CV) decreases with $\log(m)$, showing little deviation from linearity ($R^2 = 0.95$) and a regression slope close to -0.5. As compared to experimental data, showing slopes between -0.15 and -0.3, $\text{CV}_{\text{flow}}(m)$ in the model decreases more rapidly with increasing mass of sample.

[1] W. M. Chilian, personal communication, Mar. 1992.

V. Discussion

A. Critical Review of Particular Aspects

The connective structure as well as segment locations depend on the sequence of pseudorandom numbers chosen for a particular realization of the model. Especially the locations tossed for the first few terminal segments determine the "visual" appearance of the tree, since the segments generated in the early stages of development evolve to become major branches later on. Consequently, optimization can only be achieved "within" each given random number sequence. The uncertainty thus induced can be estimated from the standard deviations of mean segment radii (vertical bars in Fig. 4). These quantify the "sensitivity" of the tree's morphometric properties to changes in random number sequence.

The procedure used for "adding a terminal segment" can alternatively be interpreted as the "induction step" in a mathematical proof: first, we noted that a tree with only one segment can be balanced and scaled. Then, starting from a preexisting and balanced tree of k_{term} terminal segments, another terminal can always be added at an arbitrary connection site to obtain a balanced tree with $k_{\text{term}} + 1$ terminals. Since every binary tree can be assembled by adding terminal segments, we arrive at the interesting conclusion that—aside from any question of optimization—*every binary tree can be balanced and scaled* so as to meet the boundary conditions used in the present model.

Another aspect of optimization concerns the fact that *only connection sites* are optimized each time a segment is added. Since all upstream bifurcations have to be "balanced up to the root," so as to conform to new flow splitting, their locations are no longer optimized in a strict sense. And since most of these bifurcations supply distal subtrees, these would also require reoptimization if their inlet changes location. As a result, *all bifurcations in the tree* could be reoptimized after adding one segment only. However, since the gain proved negligible we did not adopt reoptimization as part of the regular procedure. Moreover, the migration of existing segments within tissue is an effect hardly considered realistic, especially if triggered from a remote section of the three and mediated across numerous bifurcations.

As to the assumption of vasodilation for setting perfusion flow, we note that autoregulation of blood flow [15], [29]–[32] is mainly accomplished by vasomotoric constriction at the arteriolar level, which is part of the microcirculatory black-boxes within the model. Consequently, the calibers of the arteries proximal to the site of regulation should be modeled so as to permit a flow corresponding to maximum vasdodilation.

Finally, the weak dependence of p_{term} on increasing N_{term} (Table I), indicates that trees with equal r_{root} always require about the same pressure gradient $p_{\text{perf}} - p_{\text{term}}$, regardless if they are simple or very complex. After all, complex trees perform their task of homogeneous distribution in a much more elaborate way and still do not trade this for a lot of additional resistance.

The two-dimensional form of the model is a simplification of reality, not only regarding complexity but also in concept. It is important not to interpret Fig. 3 to display a projection of a three-dimensional structure onto a plane, the model is rather "intrinsically" two-dimensional. A future extension to three dimensions will require two major developments: 1) Adaption of all geometric sections in the software to three dimensions, and 2) a new conception of the target function, since hemodynamics are different between layers of myocardium.

When comparing the pressure profiles obtained from our model with experimental results, $\gamma = 2.55$ in the bifurcation law [see (2)] indeed seems more realistic than $\gamma = 3.00$. This would imply that, as far as the larger branches are concerned, minimum pulse wave reflection is more important than the possibility of uniform shear stress. As γ approaches the value 2.00, flow velocities may become equal in all major branches, a fact which has been observed experimentally in dogs [33]. One may even speculate that γ might change over the branching orders or between subtrees, so as to induce structures different for vessels being predominantly conveying or delivering in function. In short, it becomes apparent that the choice of boundary conditions (e.g., bifurcation laws) is as important as (and closely linked to) the proper selection of the target quantity itself, as discussed by Lef\'evre [7]. The described optimization method, however, is applicable to every conceivable set of constraints and target(s). Our present aim is a detailed description of the method, illustrated by results for several specific aspects and cases.

B. Comparison With Previous Models

Most previous computer models considering *whole* coronary arterial trees adhered to a compartmental or lumped parameter approach [18], [34], [35], thereby ignoring the details of geometric structure. In other models, several features of geometric structure were introduced on a statistical basis only, by generating segment lengths and diameters randomly [36], according to distributions suggested by morphometry of real vessel systems. However, even if segment lengths and radii shrink realistically across successive bifurcations [37], the segments in such a model cannot actually be assembled to a tree of "proper" geometric sturcture [36] (e.g., featuring even distribution of flow, absence of segment-crossings). Moreover similar distributions of segment parameters do not guarantee functional similarity. Still other models were restricted to the optimization of *single bifurcations* within a given frame of boundary conditions [6].

The main differences of the present approach are as follows:

1. Details of the branching structure are fully considered to a high level of complexity.
2. Distributions of segment lengths and diameters emerge from the model rather than being plugged in.
3. The locations of bifurcations are optimized according to a target function.
4. Within the *evolutionary* approach of constructing the vessel tree, the geometric optimization of single bifurcations is linked to the optimization of *overall* connective structure (according to the same target function).

Physiologic boundary conditions are maintained throughout the development of the tree, and visual inspection of the final model indicates close resemblance to real arterial structures

(Fig. 3). Moreover, the distribution of segment radii, including the caliber of the root, proved to match experimental data.

ACKNOWLEDGMENT

The authors are indebted to Dr. Burggasser and Prof.Dr. Tschabitscher for helpful cooperation regarding coronary anatomy, in particular during the revision phase of the present paper. The calculations were performed on the IBM 3090 mainframe at the Institute for Medical Informatics, University of Vienna. The authors have to thank this institution for helpful system support and generous allowance of resources.

REFERENCES

[1] M. Zamir and H. Chee, "Segment analysis of human coronary arteries," *Blood Vessels*, vol. 24, pp. 76–84, 1987.
[2] M. Zamir and M. D. Silver, "Morpho-functional anatomy of the human coronary arteries with reference to myocardial ischemia," *Can. J. Cardiol.*, vol. 1, pp. 363–372, 1985.
[3] M. Zamir and P. Sinclair, "Roots and calibers of the human coronary arteries," *Amer. J. Anat.*, vol. 183, pp. 226–234, 1988.
[4] S. Rodbard, "Vascular caliber," *Cardiol.*, vol. 60, pp. 4–49, 1975.
[5] T. Arts, R. T. I. Kruger, W. van Gerven, J. A. C. Lambregts, and R. S. Reneman, "Propagation velocity and reflection of pressure waves in the canine coronary artery," *Amer. J. Physiol.*, vol. 237, pp. H469–H474, 1979.
[6] A. Kamiya and T. Togawa, "Optimal branching structure of the vascular tree," *Bull. Math. Biophys.*, vol. 34, pp. 431–438, 1972.
[7] J. Lefevre, "Teleonomical optimization of a fractal model of the pulmonary arterial bed," *J. Theor. Biol.*, vol. 102, pp. 225–248, 1983.
[8] F. H. Netter, *Heart: The Ciba Collection of Medical Illustrations*, 2nd. ed. New York: Thieme, 1983.
[9] Y. C. Fung, *Biodynamics: Circulation.* New York: Springer-Verlag, 1984.
[10] A. S. Popel, I. P. Torres Filho, P. C. Johnson, and E. Bouskela, "A new scheme for hierarchical classification of anastomosing vessels," *Int. J. Microcirc: Clin. Exp.*, vol. 7, pp. 131–138, 1988.
[11] J. B. Bassingthwaighte, T. Yipintsoi, and R. B. Harvey, "Microvasculature of the dog left ventricular myocardium," *Microvasc. Res.*, vol. 7, pp. 229–249, 1974.
[12] M. Zamir, "Distributing and delivering vessels of the human heart," *J. Gen. Physiol.*, vol. 91, pp. 725–735, 1988.
[13] C. E. Fröberg, *Numerical Mathematics. Theory and Computer Applications.* Menlo Park, CA: Benjamin/Cummings, 1985.
[14] J. I. E. Hoffman, R. W. Baer, F. L. Hanley, and L. M. Messina, "Regulation of transmural myocardial blood flow," *ASME J. Biomech. Eng.*, vol. 107, pp. 2–9, 1985.
[15] G. M. A. Dole and V. S. Bishop, "Regulation of coronary blood flow during individual diastoles in the dog," *Circ. Res.*, vol. 50, pp. 377–385, 1982.
[16] M. Marzilli, S. Goldstein, H. N. Sabbah, T. Lee, and P. D. Stein, "Modulating effect of regional myocardial performance on local myocardial perfusion in the dog," *Circ. Res.*, vol. 45, pp. 634–640, 1979.
[17] W. Schreiner, F. Neumann, Ch. Nanninga, W. Mohl, and E. Wolner, "A computer model of myocardial squeezing and intramyocardial flow during graded coronary artery stenosis in the presence of coronary sinus interventions," *Cybernet. Syst.*, vol. 20, pp. 453–487, 1989.
[18] W. Schreiner, F. Neumann, and W. Mohl, "The role of intramyocardial pressure during coronary sinus interventions: A computer model study," *IEEE Trans. Biomed. Eng.*, vol. 37, pp. 956–967, 1990.
[19] W. M. Chilian, S. M. Layne, E. C. Klausner, C. L. Eastham, and M. L. Marcus, "Redistribution of microvascular resistance produced by dipyridamole," *Amer. J. Physiol.*, vol. 256, pp. H383–H390, 1989.
[20] W. M. Chilian, C. L. Eastham, and M. L. Marcus, "Microvascular distribution of coronary vascular resistance in beating left ventricle," *Amer. J. Physiol.*, vol. 251, pp. H779–H788, 1986.
[21] S. H. Nellis, A. J. Liedtke, and L. Whitesell, "Small coronary vessel pressure and diameter in an intact beating rabbit heart using fixed-position and free-motion techniques," *Circ. Res.*, vol. 49, pp. 342–353, 1981.
[22] H. Tillmanns, M. Steinhausen, H. Leinberger, H. Therderan, and W. Kubler, "Pressure measurements in the terminal vascular bed of the epimyocardium of rats and cats," *Circ. Res.*, vol. 49, pp. 1202–1211, 1981.
[23] W. M. Chilian, S. M. Layne, and S. H. Nellis, "Microvascular pressure profiles in the left and right coronary circulations," in *Coronary Circulation: Basic Mechanism and Clinical Relevance*, F. Kajiya, G. A. Klassen and J. A. E. Spaan, Eds. New York: Springer, 1990, pp. 173–190.
[24] N. S. Moise, "Echocardiography," in *Canine and Feline Cardiology*, P. R. Fox, Ed. New York: Churchill Livingstone, 1988, pp. 113–156.
[25] R. Nickel, A. Schummer and E. Seiferle, *Lehrbuch der Anatomie der Haustiere III: Kreislaufsystem, Haut und Hautorgane.* Berlin Hamburg: Parey Verlag, 1976.
[26] E. M. Renkin, "Microcirculation and exchange," in *Textbook of Physiology, Vol. 2*, H. D. Patton, A. F. Fuchs, B. Hille, A. M. Scher and R. Steiner, Eds. Philadelphia: Saunders, 1989, pp. 860–878.
[27] J. B. Bassingthwaighte, M. A. Malone, T. C. Moffett, R. B. King, S. E. Little, J. M. Link, and K. A. Krohn, "Validity of microsphere depositions for regional myocardial flows," *Amer., J. Physiol.*, vol. 253, pp. H184–H193, 1987.
[28] J. B. Bassingthwaighte, R. B. King, and S. A. Roger, "Fractal nature of regional myocardial blood flow heterogeneity," *Circ. Res.*, vol. 65, pp. 578–590, 1989.
[29] W. L. Joyner and M. J. Davis, "Pressure profile along the microvascular network and its control," *Fed. Proc.*, vol. 46, pp. 266–269, 1987.
[30] W. M. Chilian, C. L. Eastham, S. M. Layne and M. L. Marcus, "Small vessel phenomena in the coronary microcirculation: Phasic intramyocardial perfusion and coronary microvascular dynamics," *Prog. Cardiovasc. Dis.*, vol. 31, pp. 17–38, 1988.
[31] J. Rouleau, L. E. Boerboom, A. Surjadhana and J. I. E. Hoffman, "The role of autoregulation and tissue diastolic pressure in the transmural distribution of left ventricular blood flow in anesthetized dogs," *Circ. Res.*, vol. 45, pp. 804–815, 1979.
[32] A. K. Ellis and F. J. Klocke, "Effects of preload on the transmural distribution of perfusion and pressure flow relationships in the canine coronary vascular bed," *Circ. Res.*, vol. 46, pp. 68–77, 1980.
[33] Y. Koiwa, R. C. Bahn, and E. L. Ritman, "Regional myocardial volume perfused by the coronary artery branch: estimation in vivo, *Circulation*, vol. 74, pp. 157–163, 1986.
[34] Y. Sun and H. Gewirtz, "Estimation of intramyocardial pressure and coronary blood flow distribution," *Amer. J. Physiol.*, vol. 255, pp. H664–H672, 1988.
[35] P. Bruinsma, T. Arts, J. Dankelman and J. A. E. Spaan, "Model of the coronary circulation based on pressure dependence of coronary resistance and compliance," *Bas. Res. Cardiol.*, vol. 83, pp. 510–524, 1988.
[36] J. H. G. M. van Beek, S. A. Roger and J. B. Bassingthwaighte, "Regional myocardial flow heterogeneity explained with fractal networks," *Amer. J. Physiol.*, vol. 257, pp. H1670–H1680, 1989.
[37] G. Pelosi, G. Saviozzi, M. G. Trivella, and A. L'Abbate, "Small artery occlusion: A theoretical approach to the definition of coronary architecture and resistance by a branching tree model," *Microvasc Res.*, vol. 34, pp. 318–335, 1987.
[38] H. H. Lipowsky and B. W. Zweifach, "Methods for the simultaneous measurement of pressure differentials and flows in single unbranched vessels of the microcirculation for rheological studies," *Microvasc. Res.*, vol. 14, pp. 345–361, 1977.

Wolfgang Schreiner was born June 24, 1954 in Vienna. He studied physics and mathematics and received the Ph.D. in physics in 1979 from Vienna University.

He worked on the computer simulation of liquids, first as a research fellow at London University and then as assistant at the institute for Experimental Physics at Vienna University. He was coauthor on a monography in the field of nuclear medicine. Since 1984 he has been head of the section for computerized analysis of medical data at the Second Department of Surgery, University of Vienna. 1990 he became associate professor of medical informatics and was 1991 appointed head of a working group for biomedical computer simulation.

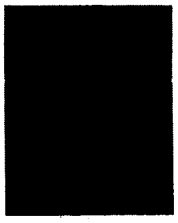

Peter Franz Buxbaum was born on September 24, 1957 in Vienna. He studied medicine at the University of Vienna and graduated as medical doctor on November 24, 1983.

He was a fellow in trauma surgery at the Lorenz Böhler Trauma Center Vienna in March 1984, then switched to the Department of Pathological Anatomy of the University of Vienna in April 1984. He worked as tutor in teaching students as well as clinical assistant in pathological diagnostics until May 1987. His scientific research concentrated in molecular biology and transplation pathological projects.

In Summer 1985 he served in the army.

Since 1985 he has been an associated pathologist at the Department of Experimental Surgery of the II Surgical Department of the University of Vienna being predominantly engaged in the construction of the Vienna artificial heart.

From May until November 1987 he worked as clinical fellow at the Cardiological Department of the University of Vienna.

In November 1987 he returned to the Department of Pathological Anatomy until April 1988, then became clinical fellow at the II Surgical Department of the University of Vienna, where clinical routine concentrated primarily in cardiovascular and throacic surgery.

From September 1990 until September 1991 he was in charge of the heart and heart–lung transplantation program of this department.

At the institution he was engaged in a wide range of scientific research projects, e.g., transplantation immunology, post transplantation medical as well as surgical problems, post transplantation cardiac-electrophysiology, laser surgery, homografting, cell-seeding of vascular prostheses, biostatistics etc.

From October 1991 until March 1992 he was at the Lorenz Böhler Trauma Center Vienna as clinical fellow, then returned to the II Surgical Department of the University of Vienna.